Tryptophan-rich basic protein (WRB) mediates insertion of the tail-anchored protein otoferlin and is required for hair cell exocytosis and hearing

C. Vogl[1,2,*], I. Panou[1,2,3,*], G. Yamanbaeva[2,4,*], C. Wichmann[1,2,5,*], S. Mangosing[6,*], F. Vilardi[7,*], A.A. Indzhykulian[8,*], T. Pangršič[2,9,*], R. Santarelli[10], M. Rodriguez-Ballesteros[11], T. Weber[1], S. Jung[1,12], X. Wu[8], S.M. Wojcik[13], K.Y. Kwan[14], I. del Castillo[11], B. Schwappach[7], N. Strenzke[2,4], D.P. Corey[8,§], S-Y. Lin[6,§], and T. Moser[1,2,12,15§]

Appendix

Table of Contents

Appendix Methods

Generation of the *Wrb* mouse line. To generate the conditional targeting vector, ET recombination (recombineering) was used to obtain a genomic fragment of the *Wrb* gene and to insert the appropriate DNA elements. A ~12.6 kb region containing exons 1-4 of the mouse *Wrb* gene was obtained from a BAC clone. This fragment was first placed into a 2.4 kb ampicillin-resistant vector backbone. The plasmid was further modified by inserting a single loxP site before exon 2 and a loxP- and FRT-flanked neomycin resistance cassette after exon 4. The final ~14.3 kb targeting vector contained 8 kb and 1.95 kb homologous arms with loxP sites flanking *Wrb*

exons 2-4 and loxP and FRT sites flanking the neomycin resistance cassette (Fig S2). The targeting plasmid was sequenced to validate the presence of appropriately created junctions as well as FRT and loxP recombination sites. For homologous recombination in embryonic stem (ES) cells, 10 μg of the targeting vector was linearized with NotI endonuclease and electroporated into BA1 (C57BL/6 x129 Sv/EV) hybrid ES cells. Transfected ES cells were cultured and selected in media containing 200 μg/ml of G418 until single clones appeared. Colonies were picked, expanded and used for screening clones that harbored the appropriate homologous recombination event. DNA obtained from individual G418-resistant ES clones were subjected to PCR screening using a primer that annealed to the neomycin cassette (F3: 5'-GCATAAGCTTGGATCCGTTCTTCGGAC) and a primer that annealed downstream of the 3' homologous arm (A4: 5'-GGAGTC TCAGATGAACTGGATCAGAC). PCR was accomplished by subjecting genomic ES DNA with primers and PCR mix to 35 cycles of amplification by denaturing at 94°C for 30 sec, annealing at 55°C for 30 sec and extending at 72°C for 2.5 min. Only DNA from the appropriate recombinant ES clones resulted in a 2.36 kb PCR fragment. The third loxP site located before exon 2 was also verified by PCR with two sets of primers (SDL1 and SDL2, SDL1: 5'-GGCTGTAATACTGGTGAC AAACGTG, SDL2: 5'-CCATCATGTTGACGGTGGACAGCTC, and SDL1/UN1, UNI: 5'-AGCGCATCGCCTTCTATCGCCTTC). After the initial PCR screens, the recombination of the long and short homologous arms were further confirmed by Southern blotting. For the long arm, ES cell genomic DNA were digested by NdeI and hybridized with a 596 bp probe targeting the 5' region outside of exon 1. For the short arm, DNA was digested by NcoI and hybridized with a 640 bp probe targeting 3' region after exon 4. DNA from C57BL/6 (B6), 129/SvEv (129), and BA1 (C57BL/6 x 129/SvEv) (Hybrid) mouse strains were used as wild-type controls. The correct ES-cell recombinant clones were expanded and used to generate chimeric mice that

were directly mated with a constitutively expressing Flp recombinase mouse (Tg (ACTFLPe)9205Dym) to remove the FRT-flanked neomycin resistance cassette. Germline transmission of recombinant ES clones resulted in mice harboring a copy of the *Wrb* conditional knockout allele that contained loxP sites flanking exons 2-4. *Wrb* conditional knockout mice were subsequently mated with two different transgenic Cre-recombinase mouse lines (see below).

Generation of *Vglut3-Cre* transgenic mice (Cre^{A}). Mouse mutagenesis and characterization is described in (Jung et al., 2015). In brief, the coding sequence for Cre-recombinase (Cre) was inserted in the start codon of the *Vglut3*/*Slc17a8* gene on bacterial artificial chromosome (BAC) RP24-88H21 by homologous recombination in *E. coli* (Liu et al., 2003). RP24-88H21 was obtained from the BACPAC Resources Center at the Children's Hospital Oakland Research Institute (Oakland, CA, USA), the plasmid containing the Cre coding sequence was a gift from Stefan Berger and Günther Schütz. *Vglut3-Cre* BAC transgenic mice were generated by pronuclear injection of the linearized BAC into fertilized FVB/NRj mouse oocytes. Expression of Cre from the *Vglut3-Cre* transgene was monitored by breeding the offspring of founder animals to Cre-reporter mice, which express EGFP after Cre-mediated excision of a loxP flanked stop-cassette (Nakamura et al., 2006).

Generation of *Vglut3-ires-Cre* knock-in mice (Cre^{B}). The generation of *Vglut3-Cre* mice was previously described (Lou et al., 2013)(Lou et al., 2013). Briefly, a *Vglut3-ires-Cre* mouse was made by knocking in an ires-Cre cassette 3 bases downstream of the *Vglut3* stop codon, so that expression of both Vglut3 and Cre recombinase are driven off a bicistronic mRNA. To characterize Cre expression, we crossed the *Vglut3-ires-Cre* mice with a tdTomato reporter mouse line and found reporter expression in all inner hair cells, few outer hair cells (3-5%), and some supporting and glial cells of the spiral ganglion.

Distortion product otoacoustic emissions. Distortion product otoacoustic emissions (DPOAEs) were measured and analyzed using custom-written MATLAB (Mathworks) routines, as previously described (Wong et al., 2014). A custom-made probe containing a MKE 2 microphone (Sennheiser, USA) and an MF1 speaker system (Tucker-Davis Technologies) was used to play two primary tones (frequency ratio f2/f1: 1.2) into the ear canal. The primary tones were intensity-adjusted using a custom-designed mouse ear coupler and a ¼" microphone (Brüel & Kjaer #4939) and sound attenuators (TDT System II). Otoacoustic emissions were measured after playing 5 different frequency combinations with a frequency ratio of 1.2, with f_1 being 10 dB lower than f_2. Every frequency combination was played for 32 sec and tested from 10 dB to 60 dB in 10 dB steps. The microphone signal was digitized using a TerraTec DMX 6fire USB soundcard.

Scanning electron microscopy. Cochleae were fixed for 1h at room temperature with 2.5% glutaraldehyde (Electron Microscopy Sciences) in 0.1M sodium cacodylate buffer (pH 7.4), supplemented with 2 mM $CaCl_2$, and then kept in distilled water until microdissection was carried out. Specimens were then dehydrated in graded ethanol solutions, critical-point dried from liquid CO_2 (Tousimis Autosamdri-815), mounted on aluminum SEM-mount stubs using carbon adhesive tabs (Ted Pella), sputter-coated with 5 nm platinum (Cressington 208HR) and examined using Hitachi S-4800 field-emission SEM, as previously described (Indzhykulian et al., 2013).

Electron tomography. The electron tomography from *Wrb*$^{fl/fl}$:*Cre*^{A} IHCs was essentially performed as described previously (Jung *et al.*, 2015; Vogl *et al.*, 2015; Wong *et al.*, 2014). Briefly, 250 nm sections were placed on formvar-coated copper-mesh-grids. After post-staining (as described in Materials and Methods), 10 nm gold particles (British Bio Cell International) were applied to both sides of the grids. A single axis tilt series was acquired using a JEM 2100 transmission electron

microscope (JEOL, Echingen, Germany) at 200 kV from -55° to +55° with 1° increment at 12,000x using the Serial-EM software package (Mastronarde, 2008). The tomograms were generated using the IMOD package etomo (Kremer et al., 1996). The tomogram was segmented and rendered semi automatically using 3dmod.

FM1-43 loading experiments. Organs of Corti and utricles were dissected from P7 mice in Leibovitz L-15 cell culture medium (Life Technologies) and mounted on coverslips using tungsten minutien pins. Following the medium aspiration, FM1-43 solution (2 µM in L-15) was applied to the tissue for 30s, which was then quickly aspirated, tissue rinsed once with L-15 and the excessive dye quenched by 0.2 mM solution of 4-sulphonato calix[8]arene, sodium salt (SCAS) in L-15. Tissue was then observed on an upright Olympus FV1000 confocal microscope, equipped with 60x 1.1 NA water dipping objective lens.

Whole-cell patch clamp recordings of hair cell MET currents. Organ of Corti explants were dissected at P3-P4 and cultured in glass bottom Petri dishes (WPI Inc.) for 3-5 days in DMEM/F12 medium (Life Technologies) supplemented with 5% FBS and 10 mg/l ampicillin at 37°C (10% CO_2) as previously described (Indzhykulian et al., 2013). Experiments were performed at room temperature in L-15 (Life Technologies) containing the following inorganic salts (in mM): NaCl (137), KCl (5.4), $CaCl_2$ (1.26), $MgCl_2$ (1.0), Na_2HPO_4 (1.0), KH_2PO_4 (0.44), $MgSO_4$ (0.81). Hair cells were observed with an inverted microscope (TE2000, Nikon) using a 100x 1.3NA oil-immersion objective lens and DIC optics. To access the hair cells, some of the outermost supporting cells were removed by gentle suction with a ~5 µm micropipette. Smaller pipettes for whole-cell patch-clamp recordings were filled with intracellular solution containing (in mM): CsCl (140), $MgCl_2$ (2.5), Na_2ATP (2.5), EGTA (1.0), HEPES (5.0). The pipette resistance was typically 4-6 MΩ when

measured in the bath. Patch clamp recordings were performed with an AxoPatch 200B amplifier (Molecular Devices). Hair cells were held at –60 mV between the short periods of MET recordings, when the holding potential was temporarily decreased to –90 mV. All recorded hair cells were located approximately at the middle part of the organ of Corti explant.

Hair bundles were deflected using a stiff glass probe, fire-polished to a fit the shape of the stereocilia bundle (~5-9 µm, depending on the cell type). The probe was mounted on a piezo actuator (PA 8/14 SG, Piezosystem Jena), built-in strain gauge sensor of which provided a direct reading of the probe's axial displacement. The piezo was driven by a custom-made amplifier, providing a rapid step deflection within ~40µs (10-90% of the amplitude) for the maximum amplitude used in the study. The angle between the axis of the probe movement and the bottom surface of a dish was kept constant at ~30 degrees.

Protein purification and *in vitro* post-translational membrane insertion

For pQET328-10hisZZ-OTOFop, the coding sequence of otoferlin (amino acids 1733-1997) was amplified from pEGFP-Otoferlin using the primers TATACAGGTACCGAGCTGCGGGTCATCGTGTGGAACACAGACGAG and TAGTATAAGCT

TTTAGCCCGTCTTGTTGGAGAAAGGCACGTAGAAGTTTGGGCCGGCCCCTAGG AGCTTCTT containing KpnI and HinDIII restriction sites respectively. This PCR reaction introduces a C-terminal opsin tag containing a N-glycosylation site. The fragment was cloned into pQET328-10hisZZtev (Favaloro et al., 2010). A NheI/AvrII fragment generated from pQET328-10hisZZ-OTOFop was cloned into pQE80-MBP-TRC40wt andpQE80-MBP-TRC40gr (Favaloro et al., 2010) to generate the constructs pT5L_T7-MBP-TRC40wt_hisZZ-OTOFop and pT5L_T7-MBP-TRC40gr_hisZZ-OTOFop respectively for bacterial expression of TRC40/OTOF

complexes.

Appendix Table Legends

Appendix Table S1: Fraction of failing auditory brainstem response recordings at maximal stimulation levels, related to Figure 3

Table S1 presents the percentage failure for auditory brainstem response recordings at maximal stimulation levels for *Wrb*$^{+/+}$*:Cre*^{A}, *Wrb*$^{fl/fl}$*:Cre*^{A} and *Wrb*$^{fl/fl}$ mice of the three age groups studied at a given type of stimulation (tone burst or click). Hyphen indicates no failures.

Appendix Table S2: Cell shape analysis of IHCs from otoferlin mutant mice, related to Figure S6

Analysis of cell shape in *pachanga* mice, which carry a point mutation in *Otof*. Analysis was performed as in Fig. S7 on immunohistochemical samples, prepared, imaged and published in (Pangrsic et al., 2010).

Appendix Table S3: Number of synaptic ribbons, postsynaptic AMPA receptor clusters and ribbon-occupied synapses per IHC, related to Figure 5 and Figure 6

Table S2 presents the quantification of pre- and postsynaptic specializations and ribbon-occupied synapses per IHCs obtained from counting immunofluorescent spots for RIBEYE/CtBP2 (synaptic ribbons), GluA2/3 (postsynaptic AMPA receptor clusters) and juxtaposed RIBEYE-GluA2/3 spots (ribbon-occupied synapses) in stacks of confocal sections obtained from apical coils of the organ of Corti after the onset of hearing (P14-17). No significant differences were observed between *Wrb*$^{+/+}$*:Cre*^{A}, *Wrb*$^{fl/fl}$*:Cre*^{A} and *Wrb*$^{fl/fl}$ mice.

Appendix Figure Legends

Appendix Figure S1

(A) HZZ-OTOFop was translated in a coupled transcription/translation competent rabbit reticulocyte lysate (RRL) immunodepleted of TRC40, HSC70 or in a control lysate in presence or absence of rough microsomes (RM). Reactions were separated by SDS-PAGE and analyzed by immunoblot with an opsin antibody. Asterisks (*) indicate residual TRC40 antibodies used for immunodepletion.

(B) Immunodepleted and control lysates were analyzed by immunoblot with TRC40 and HSC70 specific antibodies. GAPDH was used as loading control.

(C) HZZ-OTOFop was translated in RRL in presence of RM, trypsin treated RM or in presence of the cytosolic domain of WRB (WRBcc). Newly synthesized proteins were detected by opsin immunoblot.

Appendix Figure S2 Hair cell specific *Wrb* deletion using *Vglut3-Cre* mutants, related to Figure 3-7

(A) Apical turn of a representative P17 $Wrb^{+/+}$:Cre^{A} animal illustrating IHC-specific and homogenous expression of GFP, thereby confirming targeted Cre recombination. Cell nuclei are counterstained with DAPI.

(B) Cre-driven tdTomato expression in IHCs and few supporting cells in $Wrb^{+/-}$:Cre^{B} animals at P6. Please note that only very few OHCs express the Cre-dependent fluorescently-tagged markers in both Cre lines.

(C-C') In each patch-clamp experiment IHCs of Cre^{A} animals (in this case $Wrb^{+/+}$:Cre^{A}) were tested for GFP expression to confirm Cre-driven recombination. White arrowhead points to a Cre-expressing OHC. (C') Bright field image showing the experimental arrangement used for perforated patch experiments (patch pipette on the left). OHCs and supporting cells were

removed to gain access to the basolateral side of IHCs. GFP fluorescence is superimposed, revealing successful Cre recombination in all IHCs.

(D) *Wrb*$^{fl/fl}$*:Cre*^{A} animals on average have lower body weights as various control animals (*Wrb*$^{+/+}$*:Cre*^{A}, *Wrb*$^{fl/+}$*:Cre*^{A} or *Wrb*$^{fl/fl}$) and die within 2 months after birth. Weights of individual animals are displayed.

Scale bars: in A, B and B': 200 µm, in B'' 20 µm

Appendix Figure S3 Indications for more basolateral ER and lysosomes but largely unchanged Golgi and cuticular plate in the apical pole *Wrb*$^{fl/fl}$*: Cre*^{A} IHCs

A-B) Apical part of a wild-type C57BL/6 (P48) (A) and a *Wrb*$^{fl/fl}$*:Cre*^{A} (P24) (B) IHC. Organelles like the Golgi apparatus (blue arrows) or the cuticular plate (yellow arrows) appear unchanged. Occasionally, large vesicular structures can be observed in the mutant (read circle in B). Scale bars: 2 µm. (A) Courtesy of Susann Michanski (Institute for Auditory Neuroscience Göttingen).

A'-B') Basal region of a *Wrb*$^{+/+}$*:Cre*^{A} (P21) (A') and a *Wrb*$^{fl/fl}$*:Cre*^{A} (P21) (B') IHC. ER is found unaltered in the cytoplasm (yellow arrows), whereas the large accumulations of vesicles are only found in the mutant (red arrow in B'). Scale bars A': 1 µm; B': 500 nm.

C-C') Representative single optical sections through a central plane of P21 (C) control or (C') *Wrb*$^{fl/fl}$*:Cre*^{A} IHCs, immunostained with specific antibodies against the lysosomal marker LAMP1 (green) and otoferlin (magenta), illustrating apparently increased lysosome abundance in the mutants.

D-D') Virtual section of a tomographic reconstruction (D) with the according model (D') of a *Wrb*$^{fl/fl}$*:Cre*^{A} (P21) ribbon synapse. The arrows highlight cisternal structures (light blue) found close to the synaptic ribbon (red), which might represent hyperplastic ER. Blue: membrane; yellow: synaptic vesicles; magenta: presynaptic density. Scale bars: 200 nm.

Appendix Figure S4 Extensive IHC loss but normal OHC counts in 5 week-old *Wrb$^{fl/fl}$: Cre^{A}* animals, related to Figure 3 and EV5

(A-A') Maximum projections of 5 weeks-old (A) *Wrb$^{+/+}$:Cre^{A}* and (A') *Wrb$^{fl/fl}$:Cre^{A}* organs of Corti stained for the IHC-specific marker Vglut3 to illustrate the extensive cell loss in *Wrb* mutants at this age. Inset in (A') shows that OHCs remain unaffected in the mutants. Scale bars: 200 µm

Appendix Tables

Appendix Table S1

Group I (P14-17)								
Genotype	**ABR test frequency (% of animals with thresholds >100 dB)**							
	4 kHz	**6 kHz**	**8 kHz**	**12 kHz**	**16 kHz**	**24 kHz**	**32 kHz**	**Click 20/s**
***Wrb*$^{+/+}$*:Cre*^{A}**	37.5%	-	-	-	-	14.2%	14.2%	-
***Wrb*$^{fl/fl}$*:Cre*^{A}**	90.0%	55.0%	25.0%	15.0%	20.0%	70.0%	55.0%	-
***Wrb*$^{fl/fl}$**	86.7%	13.3%	13.3%	-	-	26.7%	33.3%	-
Group II (P21-26)								
Genotype	**ABR test frequency (% of animals with thresholds >100 dB)**							
	4 kHz	**6 kHz**	**8 kHz**	**12 kHz**	**16 kHz**	**24 kHz**	**32 kHz**	**Click 20/s**
***Wrb*$^{+/+}$*:Cre*^{A}**	-	-	-	-	-	-	-	-
***Wrb*$^{fl/fl}$*:Cre*^{A}**	100%	100%	90.0%	60.0%	40.0%	100%	60.0%	40.0%
***Wrb*$^{fl/fl}$**	-	-	-	-	-	-	-	-
Group III (>P29)								
Genotype	**ABR test frequency (% of animals with thresholds >100 dB)**							
	4 kHz	**6 kHz**	**8 kHz**	**12 kHz**	**16 kHz**	**24 kHz**	**32 kHz**	**Click 20/s**
***Wrb*$^{+/+}$*:Cre*^{A}**	25.0%	-	-	-	-	-	25.0%	-
***Wrb*$^{fl/fl}$*:Cre*^{A}**	80.0%	80.0%	80.0%	60.0%	60.0%	80.0%	80.0%	-
***Wrb*$^{fl/fl}$**	-	-	-	-	-	20.0%	40.0%	-

Appendix Table S2

Parameter	***Otof*$^{+/+}$**	***Otof*$^{Pga/Pga}$**	**Statistics**
Length of sagittal cell axis (µm)	29.3 ± 0.4	22.7 ± 0.3	p<0.001 (Wilcoxon)
Length of coronal cell axis (µm)	9.1 ± 0.1	10.0 ± 0.2	p<0.001(Wilcoxon)
Coronal/sagittal length ratio	0.32 ± 0.01	0.45 ± 0.01	p<0.001 (Wilcoxon)
Relative position of nucleus (from cuticular plate)	0.38 ± 0.01	0.40 ± 0.01	p<0.05 (*t* test)
No. of cells/organs/animals	82/7/4	64/6/4	NA

Appendix Table S3

Synapse count (Group I)			
Genotype	*Wrb*$^{+/+}$*:Cre*^{A}	*Wrb*$^{fl/fl}$	*Wrb*$^{fl/fl}$*:Cre*^{A}
# of IHCs analyzed	119	93	140
#of CtBP2 spots/IHC	10.2 ± 1.0	13.7 ± 1.5	12.6 ± 1.7
#of GluA2/3 spots/IHC	10.2 ± 1.0	17.8 ± 4.5	12.7 ± 1.8
#of synapses/IHC	9.5 ± 0.9	11.4 ± 1.8	12.2 ± 1.6

Appendix Figures

Appendix Figure S1

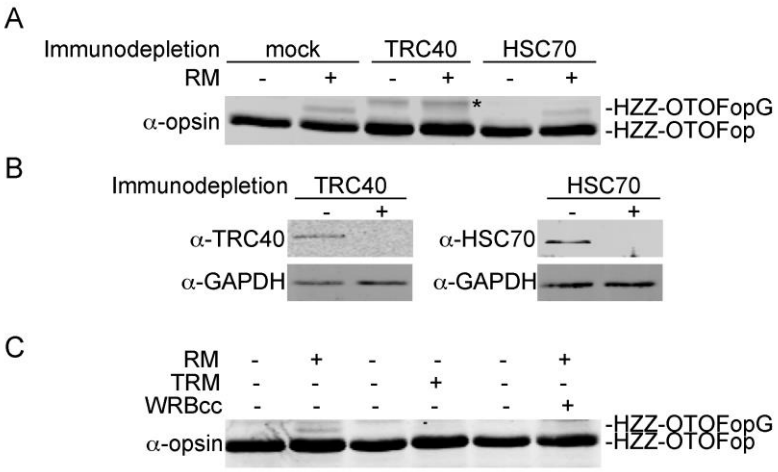

Appendix Figure S2

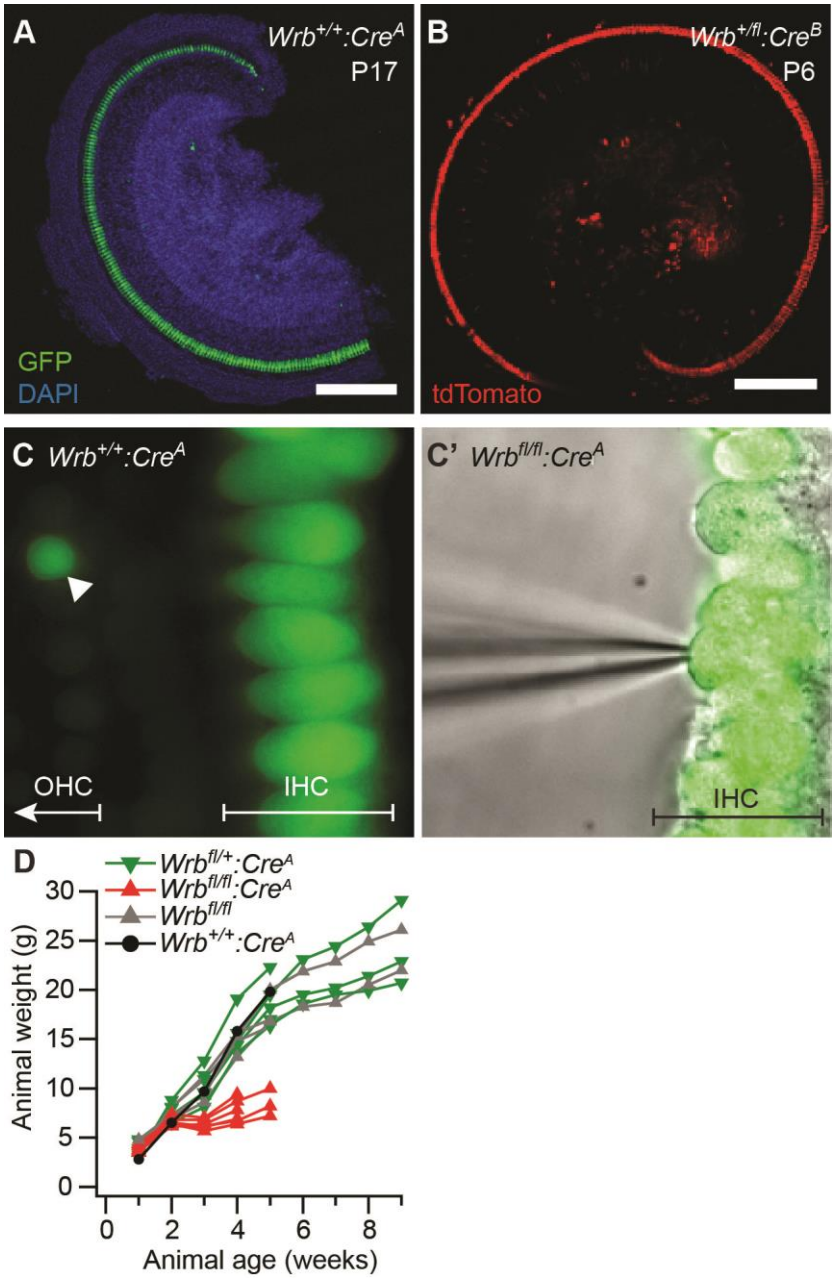

Appendix Figure S3

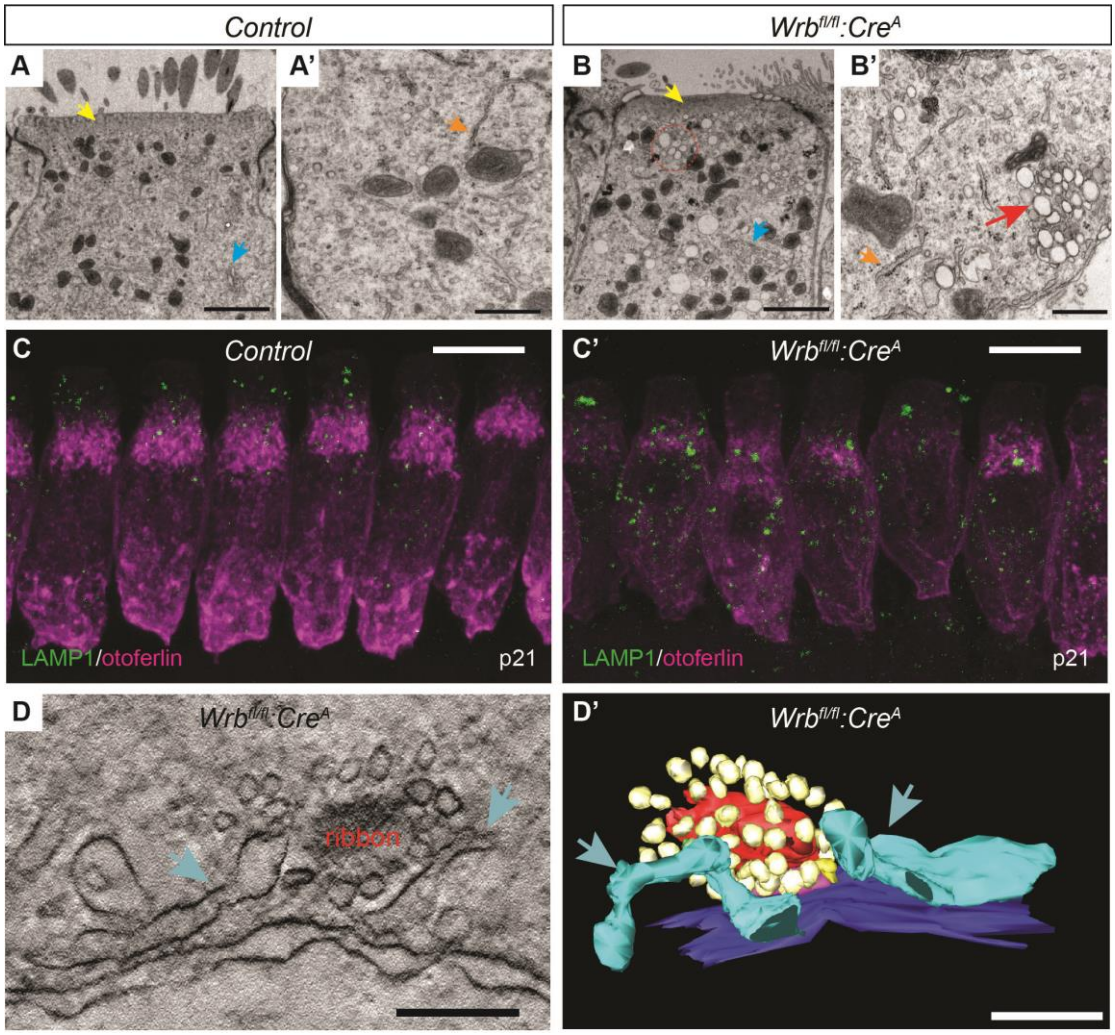

Appendix Figure S4

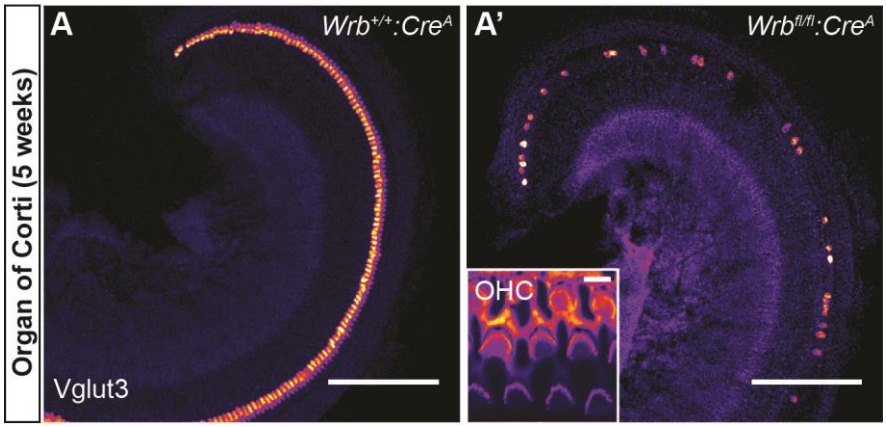

Appendix References

Indzhykulian, A.A., Stepanyan, R., Nelina, A., Spinelli, K.J., Ahmed, Z.M., Belyantseva, I.A., Friedman, T.B., Barr-Gillespie, P.G., and Frolenkov, G.I. (2013). Molecular Remodeling of Tip Links Underlies Mechanosensory Regeneration in Auditory Hair Cells. PLoS Biol *11*, e1001583.

Jung, S., Oshima-Takago, T., Chakrabarti, R., Wong, A.B., Jing, Z., Yamanbaeva, G., Picher, M.M., Wojcik, S.M., Göttfert, F., Predoehl, F., et al. (2015). Rab3-interacting molecules 2α and 2β promote the abundance of voltage-gated CaV1.3 Ca^{2+} channels at hair cell active zones. Proc. Natl. Acad. Sci. U. S. A.

Kremer, J.R., Mastronarde, D.N., and McIntosh, J.R. (1996). Computer visualization of three-dimensional image data using IMOD. J. Struct. Biol. *116*, 71–76.

Liu, P., Jenkins, N.A., and Copeland, N.G. (2003). A highly efficient recombineering-based method for generating conditional knockout mutations. Genome Res. *13*, 476–484.

Lou, S., Duan, B., Vong, L., Lowell, B.B., and Ma, Q. (2013). Runx1 controls terminal morphology and mechanosensitivity of VGLUT3-expressing C-mechanoreceptors. J. Neurosci. *33*, 870–882.

Mastronarde, D.N. (2008). Correction for non-perpendicularity of beam and tilt axis in tomographic reconstructions with the IMOD package. J. Microsc. *230*, 212–217.

Nakamura, T., Colbert, M.C., and Robbins, J. (2006). Neural crest cells retain multipotential characteristics in the developing valves and label the cardiac conduction system. Circ. Res. *98*, 1547–1554.

Pangrsic, T., Lasarow, L., Reuter, K., Takago, H., Schwander, M., Riedel, D., Frank, T., Tarantino, L.M., Bailey, J.S., Strenzke, N., et al. (2010). Hearing requires otoferlin-dependent efficient replenishment of synaptic vesicles in hair cells. Nat. Neurosci. *13*, 869–876.

Wong, A.B., Rutherford, M.A., Gabrielaitis, M., Pangršič, T., Göttfert, F., Frank, T., Michanski, S., Hell, S., Wolf, F., Wichmann, C., et al. (2014). Developmental refinement of hair cell synapses tightens the coupling of Ca^{2+} influx to exocytosis. EMBO J. *33*, 247–264.